RSC Advances

PAPER

View Article Online
View Journal | View Issue

Cite this: *RSC Adv.*, 2026, **16**, 11998

Feathered innovation: transforming recycled keratin into bioactive micro/nanoparticles for bioactive keratin-based delivery platform

Lidija Fras Zemljič, *[a] Lidija Tušek,[b] Anja Mešl,[c] Olivija Plohl,[a] Maja Čolnik[c] and Mojca Škerget[c]

At present, great importance is dedicated to the use of waste biomass for the sustainable provision and fractionation of natural resources. This is particularly true for the production of biopolymers to promote the development of novel material products based on sustainability. This growing interest is driven by socioeconomic and environmental factors. Feathers from chickens are regarded as waste from the poultry meat production sector. These organic wastes serve as natural keratin sources for synthesizing nanoparticles to develop a new generation of multifunctional biocomposites for drug delivery purposes. Thus, in this research keratin was isolated from feathers by extraction in subcritical water (SubCW) at 180 °C, 20 bar for 1 h. This recycled keratin was used to develop advanced keratin-based particles. The aim of this study was to explore the potential of subcritically extracted keratin to form electrostatically stabilized particles with different types of interaction agents—namely natural polyelectrolytes and a multivalent ionic crosslinker (TPP)—and to evaluate their performance as a multifunctional keratin-based delivery platform. To investigate the complexation ability of keratin, three polyelectrolytes with different functional groups were used for particle synthesis at specific pH values, namely alginate with carboxyl groups, chitosan with amino groups, and penta-ionic sodium tripolyphosphate (TPP) with phosphate groups. Dynamic Light Scattering (DLS) analysis showed that complex formation between keratin-alginate and keratin-chitosan resulted in microparticles, and colloidal particles were formed only in the case of keratin-TPP. The ATR-FTIR spectra of the particles indicate that electrostatic interactions were the driving force for the complex formation between keratin and oppositely charged polyelectrolytes. The antioxidant activity of keratin diminishes upon the incorporation of alginate, chitosan, and TPP. The keratin-TPP particles, identified as optimal, underwent additional assessment as a keratin-based delivery platform for the model drug amoxicillin. UV/VIS spectroscopy indicated the successful encapsulation of amoxicillin (encapsulation efficiency of 69%), with a gradual release reaching up to 96% over a 6-hours period. Antimicrobial examination showed that the increased inhibition against both *E. coli* and *S. aureus* in the keratin-based delivery platform compared to pure amoxicillin can be attributed to the successful and controlled release of the drug from the particles. Consequently, these particles exhibit promising potential as a delivery system, offering simultaneous antioxidant and potentially antimicrobial properties. The potential resistance of amoxicillin is acknowledged, but amoxicillin remains a relevant model drug for initial exploration of keratin-based delivery platforms. Further studies may explore the combination with other antibiotics for enhanced efficacy. The safety and purity of SubCW-extracted keratin are assured as it undergoes rigorous analysis, including SDS-PAGE and FTIR spectroscopy.

Received 23rd December 2025
Accepted 20th February 2026

DOI: 10.1039/d5ra09952h

rsc.li/rsc-advances

Introduction

Worldwide, the poultry meat processing industry produces several million tons of waste feathers every year.[1–3] The feathers, which are natural fibrous material, are considered waste and only small amounts are processed into valuable products such as feather meal for livestock and fertilisers. Approximately 400 million chickens are slaughtered worldwide every week, each providing ~125 grams of feathers on average, resulting in

[a]University of Maribor, Faculty of Mechanical Engineering, Institute of Engineering Materials and Design, Smetanova 17, SI-2000 Maribor, Slovenia. E-mail: lidija.fras@um.si

[b]Scientific Research Centre Bistra Ptuj, Slovenski trg 6, SI-2250 Ptuj, Slovenia

[c]University of Maribor, Faculty of Chemistry and Chemical Engineering, Smetanova 17, SI-2000 Maribor, Slovenia

~3000 tons of feather waste per week.[4] The total feather waste generated annually worldwide exceeds 18 million tons (equivalent to 4 billion pounds), of which 3.6 million tons are produced in Europe alone.[5] Conventional disposal methods such as landfilling and incineration release keratin-degrading microflora that can disrupt soil ecology and contaminate groundwater. Incineration generates CO_2 and other pollutants, while anaerobic conditions in landfills produce methane. The accumulation of unprocessed waste also fosters the buildup of pathogens, which are associated with diseases such as fowl cholera and mycoplasmosis.[4,6] In contrast, feathers are ~90% keratin, a strong, biodegradable protein with numerous potential uses. As such, keratin is a promising protein reservoir and has attracted significant attention for its biocompatibility and biodegradability.[7] However, it is still challenging to recycle feathers.

Historically, most technologies for recycling keratin from biomass waste have been harmful, expensive, toxic, and difficult to handle.[8–13] Keratin can be extracted using several approaches such as chemical hydrolysis, enzymatic and microbial treatment, dissolution in ionic liquids, microwave technique, steam explosion and thermal hydrolysis or a superheated process.[7] Conventional extraction refers primarily to commonly used chemical keratin isolation routes including alkaline/reductive dissolution (*e.g.*, NaOH/urea with reducing agents such as sulfide, thioglycolate, β-mercaptoethanol or DTT) and oxidative or sulfitolysis treatments (*e.g.*, peracetic acid or sulfite/metabisulfite), which typically rely on harsh reagents and extensive downstream purification. These methods may also cause molecular degradation (*e.g.*, amino-acid degradation at elevated temperatures).[14] Enzymatic hydrolysis, which is considered to be environmentally safe and cost-effective, is carried out under the influence of certain reducing agents which can destroy keratin's disulphide bonds.[15] Dissolution in ionic liquids and microwave irradiation yield low keratin concentrations.[15] These processes are time-consuming and have not evolved significantly over the years despite technological advancements. Moreover, mentioned extraction methods often produce lower molecular weight keratin and limited solubility, making it unsuitable for certain applications. Therefore, it is essential to develop new and more efficient extraction technologies that minimize molecular degradation while preserving functional properties, especially for biomedical use.

Subcritical water (SubCW) has gained increasing attention as both an environmentally friendly solvent and a highly attractive reaction medium for various applications. SubCW is inexpensive, non-toxic, non-flammable, and non-explosive, offering essential advantages compared to other chemicals, particularly in the field of "green chemistry".[16] SubCW provides a high yield of keratin (up to 90.5% at 200 °C), which makes it superior to conventional alkaline and acidic treatments, which yield lower amounts of more degraded proteins.[17] Reaction time and temperature can be adjusted to maximize molecular weight and yield and minimize excessive protein degradation. The keratin is extracted with intact chemical and secondary structure, and the hydrolysate is colloidal and ready for biomedical formulations.[17,18] In our previous work, SubCW was successfully applied for the extraction of keratin from keratin-rich substrates such as waste wool and poultry feathers, demonstrating its versatility.[18,19] However, systematic research into the applicability of keratin isolated by hydrothermal processing has not yet been extensively explored, and its use as a carrier system remains underreported. This study, therefore, extends this research by investigating the formation of keratin-based nanoparticles, while preserving high yields and functional properties. At present, the global market for keratin-based materials is rapidly expanding across industries such as hair care, cosmetics, personal care, medicine, and food products. The keratin market is projected to grow at a rate of 7.30% during the forecast period from 2022 to 2029, with an expected market value of USD 1.96 billion by 2029.[20]

The complexation of keratin with various compounds has been explored for biomedical and cosmetic applications, leading to the introduction of new functionalities. Recent research has focused on combining keratin with other compatible materials, with a growing emphasis on the use of natural polymers to address environmental concerns associated with plastics. Among the most promising approaches are the blends of keratin with biodegradable materials such as fibroin and sericin (proteins derived from silk) for wound healing and tissue regeneration.[21] Similarly, cellulose derivatives and biodegradable polyesters like PLA and PCL are increasingly used in biomedical scaffolds and keratin-based delivery platforms.[22–24] These developments reflect a shift toward fully bio-based functional delivery systems, emphasizing the need for systematic comparisons between various polymeric complexation strategies.[25]

Chitosan is a positively charged polymer that can form complexes with keratin *via* interfacial electrostatic interactions, resulting in polyelectrolyte complexes and microcapsule formation.[26] In most reported systems, however, chitosan–keratin composites are stabilised by additional crosslinking steps using agents such as glutaraldehyde, genipin or photo-induced reactions.[26–29] In contrast, the present study focuses on the direct electrostatic complexation of the two biopolymers in the absence of external crosslinkers, in order to preserve biocompatibility and simplify the formulation workflow.

Alginate, a negatively charged natural polysaccharide, can also form complexes with keratin and is widely used in drug delivery due to its biocompatibility, mucoadhesiveness, swelling capacity, sol/gel transition behaviour and favourable mechanical properties.[30,31] Its anionic carboxylate groups provide a complementary partner for cationic sites on keratin, enabling the formation of ionically crosslinked structures that are attractive for controlled release formulations.

Sodium tripolyphosphate (TPP), a small multivalent anion, is a well-established ionic crosslinker in chitosan-based keratin-based delivery platforms, where it promotes the formation of stable, nanoscale particles through ionotropic gelation.[32–38] In this study, TPP is investigated as an interaction partner for keratin, representing a novel crosslinking strategy for keratin-based carriers. To the best of our knowledge, the use of keratin-TPP particles for drug encapsulation with amoxicillin

has not yet been systematically evaluated and therefore warrants detailed investigation.

The use of keratin-TPP particles for drug encapsulation with amoxicillin has not yet been systematically evaluated in relevant literature and warrants further investigation. Our study contributes to this evolving field by comparing keratin complexation with a synthetic ionic crosslinker (TPP) and natural polyelectrolytes (alginate, chitosan), aiming to explore their structural, bifunctional, and drug delivery behaviour in a unified framework. Overall, these three interaction partners were selected to represent complementary formulation strategies for keratin-based drug carriers: (i) a small multivalent ionic crosslinker (TPP) to condense keratin into compact nanoscale particles and potentially slow diffusion-driven release, (ii) a cationic polyelectrolyte (chitosan) to form polyelectrolyte complexes, strengthen the carrier structure and provide mucoadhesive/antibacterial-relevant surface charge, and (iii) an anionic polyelectrolyte (alginate) to form hydrophilic complexes that can modulate swelling and diffusion, relevant for sustained topical delivery. This comparative framework enables us to link the choice of interaction agent with particle size, surface charge, colloidal stability and release behaviour.

To address this, the present work investigates and compares the formation of three types of keratin-based particles—keratin-TPP, keratin-alginate and keratin-chitosan—using keratin extracted *via* SubCW. Among these, only the keratin-TPP system was further explored for drug delivery, with amoxicillin used as a model antibiotic. The study evaluates the physicochemical characteristics and antioxidant properties of all complexes and specifically assesses the encapsulation and release behaviour of keratin-TPP-based particles. Through this comparative framework, the study seeks to identify structure–function relationships and assess the practical applicability of keratin complexes in wound treatment platforms such as hydrogels or bioadhesive films. This highlights the unique behaviour of SubCW-derived keratin, which differs from typical keratin obtained by chemical extraction, and provides the first direct comparison of keratin complexation with alginate, chitosan and TPP under an identical formulation protocol. Unlike conventionally extracted keratin, SubCW-derived keratin retains higher molecular integrity and preserves key secondary structures (Amide I/II), making it a promising candidate for particle engineering. This is expected to directly affect complexation-driven particle formation, since electrostatic assembly depends on the availability and distribution of ionisable groups and on sufficient chain length for multivalent interactions. In our previous work,[18] SubCW keratin showed a polymeric MW fraction ($\approx$4.6–15 kDa) and amphoteric charge behaviour (IEP $\approx$ 4.3–4.4), which enables pH-tunable interactions with oppositely charged polyelectrolytes and multivalent anions, thereby impacting particle size and colloidal stability.

Experimental

Materials

Fresh poultry feathers were obtained from a local slaughterhouse (Perutnina Ptuj d.d., Ptuj, Slovenia) immediately after processing and cleaned (were thoroughly washed with warm water and a mild non-ionic detergent to remove lipids, dirt, and microbial residues, following the standard cleaning procedure previously reported in the literature[18]) and stored at 4 °C and processed within 72 h to prevent microbial degradation. Sodium tripolyphosphate (TPP), sodium alginate (medium viscosity), and chitosan (medium molecular weight, 75–85% deacetylated) were purchased from Sigma-Aldrich (Merck KGaA, Darmstadt, Germany). Amoxicillin trihydrate ($\geq$95%) was supplied by Kemika d.d. (Zagreb, Croatia). All chemicals were of analytical grade and used as received without further purification. Deionised water (resistivity $\geq$ 18.2 MΩ cm, Milli-Q, Millipore) was used in all experiments.

Subcritical water extraction of keratin

A 75 mL high-temperature, high-pressure batch reactor (series 4740 Stainless Steel, Parr Instruments, Moline, IL, USA) was used to extract keratin from feathers with SubCW. Poultry feathers were subjected to SubCW extraction under conditions found to be optimal for obtaining a high molecular weight protein hydrolysate from poultry feathers in our previous study,[18] namely at 180 °C, 20 bar for 1 h. Most of the feathers decomposed, resulting in a water-based suspension. After extraction, the suspension was subjected to a freeze-drying process. The procedure is described in detail in our previous publications.[18,19]

Preparation of keratin-based micro/nanoparticles

The complexation and preparation of the particles was done by adding the polyelectrolyte solutions (1% alginate, 1% chitosan and 0.1% tripolyphosphate TPP, respectively) dropwise to the 5.5% aqueous suspension of recycled keratin at 30 °C during constant stirring for 30 min. The suspensions were centrifuged twice, *i.e.* first at 8000 rpm for 5 min and then at 9000 rpm for 10 min, until the dispersion was clear. These will hereafter be referred to as "keratin-based particles" for clarity and consistency.

The pH during particle formation was adjusted using diluted HCl or NaOH, without the use of buffer systems, to avoid interference with ionic interactions. This ensured that keratin and the interaction agents remained in their charged states suitable for electrostatic complexation. No visible flocculation occurred during pH adjustment or mixing, and the suspensions remained colloidally stable throughout synthesis. This was likely due to the low keratin concentration and controlled pH environment. The initial keratin concentration in the solution was 5.5% w v^{-1}. Following centrifugation and particle isolation, less than 5% of the keratin was found in the supernatant, indicating that the majority was successfully incorporated into the particles.

Alginate and TPP enabled ionic interactions with the amino groups of keratin and the anionic groups of alginate (carboxyl group) and TPP (phosphate group), respectively. The complexation process was carried out at a pH value of 4. This pH was chosen based on findings from our prior research,[18] which demonstrated that the zero-charge point (isoelectric point) of

the keratin suspension occurs at a pH of 4.3. Below this pH value, the solution displays a positively charged character due to the presence of protonated amino groups in the keratin. Conversely, above the isoelectric point, the solution exhibits a negative charge, attributed to deprotonated carboxyl groups, resulting in a negative zeta potential. For the complexation between keratin and chitosan, ionic interactions were expected to occur between the protonated amino groups of chitosan (isoelectric point was determined to be in the pH range between 6.3 and 6.7 as determined in the previous work[39]) and the deprotonated carboxyl groups of keratin. To make sure that both groups are partly charged, a pH of 5.5 was selected for synthesis of the particles.

Characterisation of the particles

The hydrodynamic diameter of the particles by means of dynamic light scattering (DLS) of the prepared dispersions/suspensions in aqueous systems was characterised using the Litesizer 500 DLS by Anton Paar.

Zeta potential measurements through electrophoretic light scattering (ELS) were performed in Omega cuvette using the same instrument in Milli-Q water at 25 °C. The pH of the keratin suspension was adjusted using diluted HCl or NaOH. The isoelectric point was determined by plotting zeta potential as a function of pH. For comparison of the three keratin-based systems, the zeta potential of keratin-alginate and keratin-TPP particles was measured at pH 4.0, while keratin-chitosan particles were measured at pH 5.5. These pH values were selected based on the isoelectric point of keratin (pH 4.3), ensuring that both keratin and the interacting polyelectrolytes carried the appropriate charge for electrostatic complexation.

Infrared spectra were obtained using the Pelkin Elmer Spectrum GX NIR FT-Raman spectrometer (Waltham, MA; USA) equipped with a diamond crystal ATR accessory, operating in transmission mode. Initially, a background spectrum was recorded, followed by measurements of the samples using identical parameters. The measurement conditions included 30 scans with a resolution of 4 cm^{-1} over the wavenumber range of 4000–400 cm^{-1}. Subsequently, the obtained spectra underwent smoothing *via* automatic smoothing filters, automatic baseline corrections, and ATR corrections, before being normalized to 1 for comparative analysis. In the absence of a common reference band across all samples, spectra were baseline-corrected and normalized using a consistent whole-spectrum approach for visualization. All measurements were conducted at room temperature.

Drug encapsulation efficiency

Amoxicillin was added directly into the keratin solution prior to TPP-induced complexation. During particle formation, the drug became encapsulated within the keratin-TPP matrix. Free (unencapsulated) amoxicillin was then removed *via* centrifugation. The concentration of encapsulated amoxicillin was determined by analysing the supernatant with UV-Vis spectroscopy. The drug encapsulation efficiency (EE) was indirectly determined following the separation of keratin-TPP-amoxicillin nanoparticles from the medium containing non-encapsulated amoxicillin using a centrifugation-based technique. The percentage of amoxicillin encapsulation efficiency in the nanoparticles was measured using UV-Vis spectrophotometry at 273 nm (Cary 60 UV-Vis spectrophotometer, Agilent Technologies, Santa Clara, CA, USA) and calculated as follows:

$$\text{Encapsulation efficiency (\%)} = (c_{\text{initial}} - c_{\text{in the supernatant}})/c_{\text{initial}} \times 100\%$$

where c_{initial} is the concentration of the amoxicillin prior to the encapsulation procedure, $c_{\text{in the supernatant}}$ is the concentration of amoxicillin in the centrifugated supernatant.

In vitro drug release testing

In vitro drug release studies were conducted using an Automated Transdermal Diffusion Cells Sampling System (Logan System 912-6, Somerset, KY, USA). The drug-loaded nanoparticles keratin-TPP-amoxicillin (centrifugated) were put in 10 mL with Phosphate Buffered Saline (PBS, purchased from Sigma-Aldrich, Germany) with a pH value of 7.4, and its temperature was maintained at 37 °C. During the dissolution testing, the medium was continuously stirred with a magnetic bar. Samples were collected over a period of 24 hours at different time intervals (0, 20, 40, 60, 80, 100, 140, 180, 220, 260, 300, and 360 minutes), while the released/dissolved amoxicillin concentration in the receptor medium was determined by a UV-Vis spectrophotometer (Cary 60 UV-Visible Spectrophotometer, Agilent, Germany) through quantification of the absorption band at 273 nm. The calculation of the concentrations was done using the Beer–Lambert Law. All release studies were performed in triplicates and are reported as the average value.

Antioxidant activity

The antioxidant activity was analysed by the spectrophotometric method using 2,2′-azino-bis-3-ethylbenzothiazoline-6-sulfonic acid (ABTS). ABTS was dissolved in water at a concentration of 7 mmol L^{-1}. The ABTS radical cation (ABTS·+) was prepared by reacting the ABTS stock solution with 2.45 mmol L^{-1} potassium persulphate (final concentration). The solution was stored overnight in the dark at room temperature. To study the antioxidant activity of the extracted solutions and the particle dispersion, the ABTS + solution was diluted with phosphate buffer solution (pH = 7.4) to obtain an absorbance of 0.700 ± 0.020 at 734 nm. Then 3.9 mL of the diluted ABTS·+ solution was added to 0.1 mL of the extracted keratin solution (as reference) or the particle dispersion. Absorbance was measured immediately, after 15 min, and after 1 h. The experiments were performed three times, and the results are given as mean values.

The percentage of radical scavenging activity (*i.e.* antioxidant activity) was determined using the equation:

$$\text{Antioxidant activity} = (A_{\text{control}} - A_{\text{sample}})/(A_{\text{control}}) \times 100\%$$

where A_{control} is the absorbance of ABTS·+ solution in phosphate-buffered saline (PBS), and A_{sample} is the absorbance

of sample (the remaining concentration of ABTS radical cation in the presence of particles).

Antimicrobial activity

The antimicrobial activity was tested using the zone inhibition test. Based on the physicochemical screening, only the optimised keratin-TPP system (with/without amoxicillin) was taken forward for antimicrobial testing. Thus, the samples tested were: (1) pure amoxicillin, (2) pure keratin, (3) keratin-TPP particles and (4) keratin-TPP particles with encapsulated amoxicillin. The sample solutions were applied aseptically to disks on solid culture media inoculated with Gram-positive *Staphylococcus aureus* (*S. aureus*) and Gram-negative *Escherichia coli* (*E. coli*) Bacteria. The incubation under optimal conditions for the growth of microorganisms at 35 °C for 24 hours followed. If the strain is susceptible to amoxicillin, a clear zone of inhibition appears around the disk, indicating the antibiotic's effectiveness against the microorganism. The size of the zone of inhibition is related to the level of antimicrobial activity of the sample.

Results and discussion

Micro/nano keratin-based particles

To give a better insight into this research, the results of the characterisation of the recycled keratin, which were described in detail in ref. 18, are also additionally summarised in this paper. Under these conditions, most of the feathers are decomposed and the keratin is extracted into a water suspension. The suspension exhibited a pH of 6.9 and a conductivity of 2.5 mS cm^{-1}. After freeze-drying of the suspension, keratin was confirmed in the solid product based on typical elemental composition examined by ATR-FTIR analysis. Molecular weight analysis *via* SDS-PAGE (Sodium Dodecyl Sulfate PolyAcrylamide Gel Electrophoresis) revealed a distribution ranging from 4.6 to 15 kDa. Zeta potential analysis demonstrated an isoelectric point at a pH of 4.3, indicating an amphoteric character. The zeta potential, within the range of 8 to −13 mV, characterized the suspension as possessing low stability, susceptible to particle aggregation, sedimentation, and flocculation. The extract itself manifested as a colloidal solution, with an average particle size of 890 nm.

To investigate the potential use of keratin obtained by SubCW extraction of chicken feathers, the recycled keratin was used in this work, to prepare keratin-based particles. These physicochemical characteristics help rationalise the particle formation behaviour observed below. The low absolute ζ-potential of the SubCW keratin hydrolysate (8 to −13 mV) indicates limited intrinsic colloidal stability, meaning that additional electrostatic complexation is required to achieve stable dispersions. Accordingly, the multivalent, low-molecular-weight TPP can form dense ionic crosslinks with oppositely charged keratin sites, yielding the smallest (nanoscale) colloidal particles. In contrast, high-molecular-weight polyelectrolytes (alginate/chitosan) tend to promote more extended and 'bridged' complexes, resulting in larger submicron-to-micron particles.

The particle size and polydispersity index of keratin-based particles blended with TPP, chitosan, and alginate, respectively, were measured using the DLS methodology. When keratin is mixed with chitosan, the results (Fig. 1) demonstrated that the resulting complexes are microparticles, while in the cases of keratin-alginate and keratin-TPP, they are colloidal particles (up to 1 micron). The size differences between these complexes may result from variations in coulombic interactions, which depend on the availability of ionised functional groups. This availability is regulated by pH, as described in the experimental section. These parameters influence the degree of cross-linking, the conformation and consequently the size of the complexes. The zeta potential values shown in Fig. 1 were obtained at pH 4 for keratin-alginate and keratin-TPP, and at pH 5.5 for keratin-chitosan, which corresponds to the ionisation states necessary for complexation (keratin IEP = 4.3). Moreover, the observed differences in particle size can be attributed to the nature of the complexing agents. The smaller dimensions of keratin-TPP particles are likely due to the low molecular weight and multivalent ionic structure of TPP, which enables tighter and denser electrostatic crosslinking with keratin. Conversely, chitosan and alginate, as a high-molecular-weight polycation, may form bulkier complexes with keratin, leading to larger particle formation.

The nanoscale size of keratin-TPP particles (<500 nm) is particularly favourable for drug delivery applications, as it enables potential penetration through the upper skin layers and supports cellular uptake. In contrast, the larger size of keratin-chitosan particles place them more in the microscale range, which may be more suitable for surface-level retention and sustained drug release on wound sites.

The relatively low polydispersity indices suggest that the particles are reasonably homogeneous in terms of size, as the polydispersity index is below 50% (33.8% in the case of keratin-alginate, 26.3% in the case of keratin-chitosan, and 25.6% in the case of keratin-TPP). The zeta potential measurements also

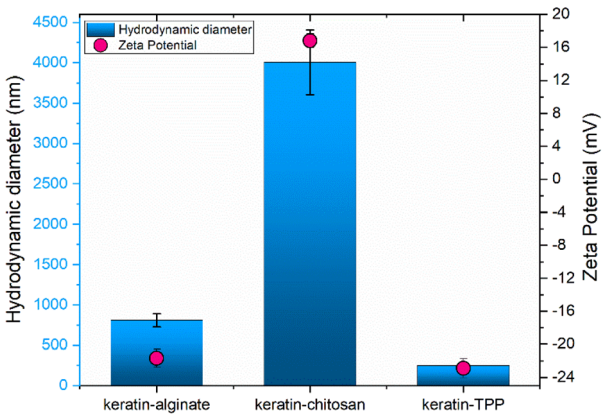

Fig. 1 Particle size and zeta potential of particles formed by complexation of recycled keratin blended with alginate, chitosan and TPP.

reveal the positive ionic character of the keratin-chitosan particles and the negative ionic character of the keratin-alginate and keratin-TPP dispersions (Fig. 1). Both anionic dispersions are relatively stable (with a zeta potential of less than −20 mV), while the cationic suspension exhibits a higher zeta potential (*i.e.* 16.8 mV) and shows a tendency towards particle agglomeration. This is one of the additional reasons why the particles in these systems are larger and escalate into the micron scale.

The negative surface charge of keratin-TPP and keratin-alginate particles indicate favourable electrostatic repulsion, which reduces the likelihood of aggregation and contributes to high colloidal stability. This is particularly advantageous for maintaining particle dispersion during storage and administration. In contrast, the positive surface charge of keratin-chitosan particles are likely due to the protonated amino groups of chitosan at acidic to neutral pH, which may enhance adhesion to negatively charged mucosal surfaces or bacterial membranes. This suggests that keratin-chitosan complexes could be more suitable for topical or transmucosal keratin-based delivery platforms. It is important to note that zeta potential is strongly pH-dependent, and further studies are needed to evaluate how surface charge responds under physiologically relevant conditions such as wound exudate (pH 6–7.5).

Overall, the variation in surface charge across the systems provides valuable insight into their prospective applications. While negatively charged systems may favour systemic dispersion or gel incorporation, positively charged particles may offer superior bioadhesive properties in localized treatment.

The presence of new peaks or the change in the shape or shifts of existing peaks in the ATR-FTIR spectra of the particles can be used to infer the formation of complexes between polyelectrolytes and keratin. Fig. 2 and 3 show the FTIR spectra of keratin, the polyelectrolyte of interest and its blended particles. Comparing the spectra of particles with the spectra of their components (Fig. 2 and 3), it can be concluded that electrostatic interactions were the driving force for the complex formation between keratin and oppositely charged polyelectrolytes.

Fig. 2a shows the FTIR spectra of keratin, alginate and a blend of keratin and alginate. The spectral peaks of keratin correspond to the peptide bonds (CO–NH) and are identified as Amide A and Amide I–III according to Sharma *et al.*[40] who published typical vibrations shown in the FTIR spectra of keratin. Stretching vibrations of O–H and N–H (Amide A) occur at 3300–3200 cm^{-1}, symmetrical –CH, $-CH_2$ and $-CH_3$ stretching vibrations occur at 3000–2000 cm^{-1}, and C=O stretching of Amide I at 1635 cm^{-1}. The vibration peak (Amide II) in the range of 1590–1470 cm^{-1} is attributed to C–H stretching and N–H bending, and the weak band at 1310–1200 cm^{-1} corresponds to Amide III band due to C–N stretching and N–H bending. The asymmetric and symmetric S–O stretching vibrations at 1076–1021 cm^{-1} indicate cysteine-S-sulfonated residues, which are formed by the reaction of sulphides and cysteine during protein extraction process.

The typical peaks in the FTIR spectra[41] of alginate are assigned to O–H stretching at 3380–3360 cm^{-1} (very strong and broad band), C–H stretching in $-CH_2$ and $-CH_3$ at 3000–2800 cm^{-1} and C=O stretching at about 1595 cm^{-1} (very strong and sharp peak) and at 1409 cm^{-1} (less strong and sharp peak). Sodium alginate exhibits a peak at 1020 cm^{-1}, which is due to the presence of C–O groups.[42]

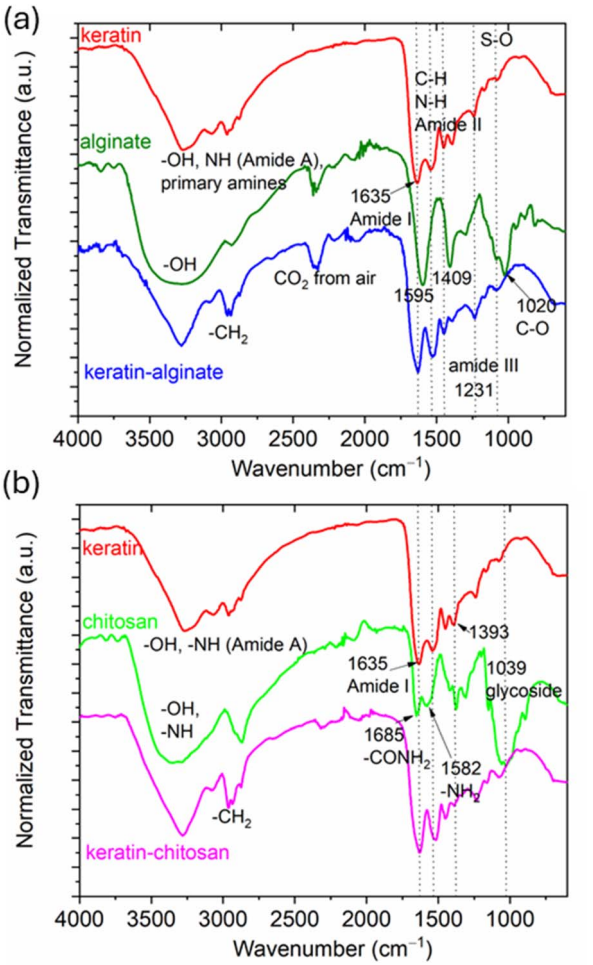

Fig. 2 ATR-FTIR spectra for keratin, alginate, and complex particles (a), and for keratin, chitosan, and its formed complex particles (b).

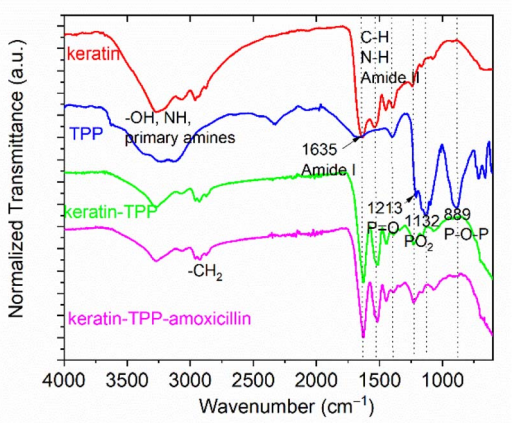

Fig. 3 ATR-FTIR spectra of a complex of keratin-TPP particles formation, further encapsulated with amoxicillin.

The bands in the spectrum of keratin-alginate are consistent with the peakss of keratin and alginate, so it is reasonable to assume that the functional groups of the particles did not change significantly during complexation. In the FTIR spectra of the keratin-alginate complex, the alginate carboxylate asymmetric stretching peak (typically observed around 1595 cm^{-1}) is less pronounced than in pure alginate. However, this attenuation likely results from overlap with the broad Amide I/II and other keratin-associated peaks, as well as possible interactions between keratin and alginate, rather than the complete disappearance of the carbonyl groups. At the same time, there are no distinct peaks in the keratin-alginate spectra associated with the primary amines/amides typically found in keratin spectra at higher wavenumbers. This change in the shape of the broad band can be attributed to electrostatic interactions with negatively charged carboxyl groups and may also be partially caused by hydrogen bonds formed.[43] Moreover, in the keratin-alginate spectrum, the alginate carboxylate peak near 1409 cm^{-1} (commonly assigned to the symmetric stretching of $-COO^-$) appears less pronounced or slightly altered in profile compared with pure alginate. This change is consistent with a modified carboxylate environment, such as ionic association or complexation with oppositely charged groups in keratin and possible band overlap in this region, supporting the formation of a keratin-alginate complex. The peak around 1020 cm^{-1} is not observed in keratin-alginate spectrum, illustrating possibility of electrostatic interaction between keratin and alginate and indicating successful cross-linking and particle formation.[44]

The functional groups of keratin-chitosan also mainly remained unchanged compared to keratin and chitosan (Fig. 2b) and are consistent with the published FTIR spectra of chitosan.[45] As in the case of alginate, the keratin-chitosan particles contain O–H and N–H bonds (peak at about 3290 cm^{-1}). Amide I occurs at about 1635 cm^{-1} for keratin and at 1685 cm^{-1} for chitosan and is present in the spectra of both keratin and chitosan components. The same is observed for Amide II band at about 1520 cm^{-1}. The peaks of the double amides in the spectrum of chitosan correspond to the partial *N*-deacetylation of chitin.[46] A peak at about 1039 cm^{-1} indicating the C–O stretching vibration for both keratin and chitosan, also occurs in the synthesised particles, but it is not so pronounced as for chitosan. The peak at around 1030 cm^{-1} in the keratin spectrum is associated with the symmetric stretching vibration of S=O in the sulfonated cysteine residue.[47] During the formation of keratin-chitosan complex particles, the spectral region associated with keratin carboxylate groups ($-COO^-$) shows relative attenuation and/or a change in peak profile in the keratin-chitosan spectrum compared with keratin alone, consistent with the involvement of oppositely charged functionalities in complexation. Because these bands arise from side-chain carboxylates[48] and are sensitive to the local electrostatic environment and hydrogen bonding, such changes are expected upon formation of a polyelectrolyte-type complex between keratin and chitosan. In addition, the Amide I peak shows some differences such as broadening/shape changes ($\sim$1635 cm^{-1}) and the absence of the $\sim$1685 cm^{-1} signal (attributed to chitosan $-CONH_2$) in the keratin-chitosan sample can be considered signs of molecular interaction, band overlap, and an altered chemical environment. Similar to the keratin-alginate complex, the keratin-chitosan particles also show changes in the shape of the broad band at higher wavenumbers. These changes can be associated with modifications of the functional groups in the keratin-chitosan system, possibly resulting from the complexation process and hydrogen bond formation. Nevertheless, the amine functional groups are retained (*i.e.*, still present), which may contribute to interactions with bacterial membranes. However, antimicrobial activity of the keratin-alginate and keratin-chitosan particles was not evaluated in this study and could be investigated in future work.

The proposed process for complexation of chitosan with isolated keratin simultaneously ensures a very strong cationic character (as revealed also by ZP results), which is highly desirable for improved antibacterial properties with respect to the keratin itself.

The characterization of the keratin particles formed with TPP and subsequently encapsulated with exemplary chosen amoxicillin was performed by ATR-FTIR spectroscopy, as shown in Fig. 3. The infrared spectrum of pure TPP showed characteristic peaks at 1213 cm^{-1} (P=O stretching), 1132 cm^{-1} (symmetric and asymmetric stretching vibrations of PO_2 groups) and 889 cm^{-1} (P–O–P asymmetric stretching).[49]

After keratin-TPP formation, the strong TPP band around 1210–1230 cm^{-1} (assigned to P=O stretching) and the bands in the 1130–1090 cm^{-1} region (phosphate O–P=O/PO_3 vibrations) appear broadened and less well resolved in the keratin-TPP particles, consistent with a distribution of phosphate binding states rather than free TPP domains. The P–O–P bridging vibration near 890 cm^{-1} (typical for TPP) is still observed but becomes weaker and less distinct, which is commonly observed[50,51] when TPP participates in ionic association or crosslinking and its local symmetry and hydrogen-bonding or ion-pairing environment changes. These spectral changes of characteristic TPP functional groups in the keratin-TPP particles suggest particle formation due to complexation between keratin and TPP. Overall, these peak-shape changes (broadening/partial masking, *etc.*), support electrostatic complexation between anionic phosphate groups of TPP and oppositely charged sites on keratin, analogous to the well-established ionotropic interactions of TPP with cationic biopolymers.[52,53] The peaks at 1635 cm^{-1} (Amide I) and Amide II, which are present in pure keratin, change their peak shape and become sharper in the keratin-TPP particles. In addition, the peaks corresponding to the functional groups for –NH and amine A in pure keratin change after particle formation with TPP, possibly indicating a reduction in available amino groups. From these spectral observations it can be suggested that effective cross-linking has occurred through ionic interactions between the negatively charged P–O– moieties of the phosphate groups of TPP and the protonated amino moieties of the keratin polypeptide chains. After encapsulation of amoxicillin in keratin-TPP particles, the spectra of keratin-TPP-amoxicillin are like those of keratin-TPP, with no new peaks emerging. This

lack of differentiation could be due to the lower concentration of amoxicillin included, which may fall below the detection limit for this spectral analysis, or to the overlap of typical functional groups of amoxicillin with peaks in the keratin-TPP spectrum. However, subsequent analyses using different methods successfully confirmed the presence of encapsulated amoxicillin.

Antioxidant activity

The antioxidant activity of keratin-based particles blended with alginate, chitosan, and TPP was analysed using the method with 2,2′-azino-bis-3-ethylbenzothiazoline-6-sulfonic acid (ABTS), which is one of the most commonly used spectrophotometric methods.[54] As expected, keratin exhibits antioxidant activity immediately, giving the absorbance at the reference wavelength of 0.082 at zero time and consequently the calculated antioxidant activity of 89% (Fig. 4). After 1 hour, the antioxidant activity is slightly higher (89%). As a control, all samples are completely discoloured (zero absorbance at 734 nm) after 4 days.

The rich sulphur content and the vulnerability of keratin to reactive oxygen species render it susceptible to oxidative damage. Nonetheless, specific compounds derived from keratin have been identified to possess antioxidant properties.[54] Key groups and compounds associated with keratin's antioxidant activity include cysteine residues, housing thiol groups (–SH) that function as antioxidants by donating electrons to neutralize free radicals.[54–56] Additionally, keratin hydrolysates, containing amino acids like cysteine and others, contribute to this antioxidant activity.[57]

Research indicates that alginate hydrolysates or alginate oligosaccharides (AOS), derived from alginate can also bolster antioxidant properties.[58] While alginate itself exhibits a modest antioxidant effect, it doesn't match the potency of other natural sources like keratin. However, when combined, certain amino and thiol groups in keratin may undergo chemical or structural modifications, potentially diminishing the antioxidant efficacy of the keratin-alginate blend. Initial measurements indicate an antioxidant activity of 2% at the onset, escalating to 42% after one hour (Fig. 4).

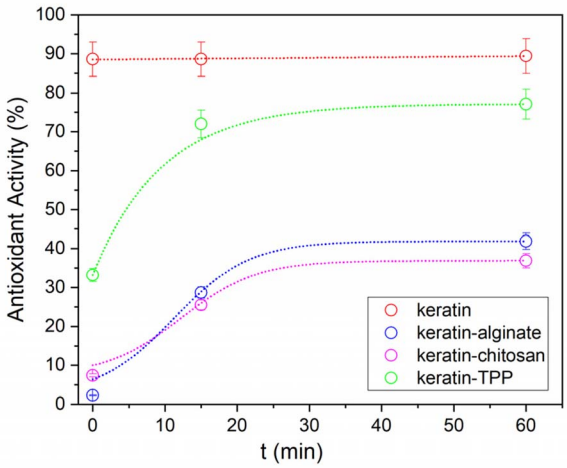

Fig. 4 Antioxidant activity of keratin-based particle formulations using ABTS assay.

Chitosan's antioxidant activity has been a subject of varied findings in research. While some studies indicate weak antioxidant effects, others report no discernible activity.[59] This variability may stem from different conditions and modifications employed to enhance chitosan's antioxidant properties, such as molecular weight, deacetylation degree, and grafting methods. Notably, chitosan nanoparticles have been shown to augment the antioxidant activity of certain compounds.[60] Challenges in demonstrating significant antioxidant effects for chitosan have been attributed to factors like poor solubility and chemical inertness due to robust hydrogen bond networks.[61] When chitosan is combined with keratin, the initial antioxidant activity is minimal (7% at zero time) but gradually escalates, reaching 37% within an hour (Fig. 4).

Several researchers have highlighted TPP as a compound capable of mitigating oxidative processes in various foods and meat products,[62,63] despite not being conventionally categorized as an antioxidant. TPP is frequently employed as a cross-linking agent and stabilizer in nanoparticles. In the synthesis of chitosan nanoparticles, TPP serves as a cross-linking agent, facilitating the formation of more stable dispersions and heightened zeta potential values, thus bolstering nanoparticle stability.[64,65] In the preparation of keratin nanoparticles, TPP is utilized in methods like desolvation and cross-linking, fostering interactions with keratin to yield stable nanoparticles.[27] The antioxidant activity of a keratin-TPP blend in Fig. 4 exhibits an initially high level (33%), rapidly escalating within the first 15 minutes to plateau at 80% after approximately 30 minutes. This may indicate that keratin-TPP nanoparticles offer improved accessibility of keratin antioxidant groups, as inferred from the combination of the fastest/highest ABTS scavenging kinetics and the nanoscale, colloidally stable particle size compared with keratin-alginate and keratin-chitosan complexes.[66,67] The formation of compact nanoscale particles upon addition of a small multivalent polyanion such as TPP is consistent with the ionotropic crosslinking/gelation mechanism reported for TPP-based nanoparticles.[68]

The preserved antioxidant activity suggests that the keratin matrix retains its intrinsic bioactivity post-complexation, which is essential in oxidative wound environments. This aligns with prior studies: for example, keratin hydrolysates demonstrated strong radical scavenging ability in ABTS and DPPH assays, achieving up to 77% inhibition and inhibiting Fe^{2+}-induced degradation of hyaluronic acid.[69] Similarly, microparticles derived from feather keratin exhibited IC_{50} values of 5.60 μg mL^{-1} in ABTS assays, underscoring their significant antioxidant potential.[70]

This indicates that the keratin-TPP nanoparticles possess a structural arrangement that preserves and exposes a greater number of keratin's antioxidant functional groups, in contrast to the denser, less accessible matrices formed with alginate and chitosan, making keratin-TPP the most promising candidate for an effective multifunctional keratin-based delivery platform. This function is particularly relevant in wound healing, as chronic wounds are characterized by elevated levels of reactive

oxygen species (ROS), which can damage cells and extracellular matrix, impeding the healing.[71] By scavenging ROS locally, keratin-based particles may help normalize redox balance and support tissue regeneration.

Keratin-based delivery platform keratin-TPP-amoxicillin

The keratin-TPP nanoparticles, which proved to be the optimal combination with keratin among all polyelectrolytes used, were further tested as a keratin-based delivery platform for the model drug amoxicillin. Amoxicillin is a widely used antibiotic that is effective against a wide range of bacteria, including Gram-positive and some Gram-negative organisms[55] It is recommended for the treatment of infections resulting from susceptible isolates of bacteria, particularly those that are beta-lactamase-negative. These infections include infections of the nose, throat, and ears, elimination of *Helicobacter pylori*, lower respiratory and urinary tract infections, acute bacterial sinusitis, and infections of the skin and other body structures.

UV/VIS spectroscopy was used to calculate the concentration of encapsulated amoxicillin in keratin-TPP nanoparticles. Although amoxicillin is associated with increasing β-lactamase-mediated resistance, in this study it served solely as a model compound due to its well-defined analytical behaviour and suitability for evaluating electrostatic complexation and release kinetics. Future research will extend this platform to alternative antibiotics with lower resistance rate such as fluoroquinolones or glycopeptides, to enhance its clinical relevance, enabling broader clinical applicability.[72–74] After the encapsulation process, the concentration of amoxicillin remaining in the solution was 0.1855 mmol L^{-1} or 30.8% with respect to the initial concentration of 0.6030 mmol L^{-1}. Amoxicillin was successfully encapsulated in keratin-TPP nanoparticles with an encapsulation efficiency of 69.2%. The encapsulation of amoxicillin is presumed to occur through a combination of electrostatic interactions between the protonated amino groups of keratin and the anionic β-lactam structure of the drug, as well as physical entrapment within the TPP-induced matrix network. These interactions likely contribute to the moderate but stable encapsulation efficiency observed.[75]

In the next step the kinetics of amoxicillin release from keratin-TPP-amoxicillin particles was studied (Fig. 5).

The drug release was determined by measuring the UV/VIS absorbance at 273 nm over time. Fig. 5 shows the concentration of released amoxicillin expressed as a percentage of the initial concentration of encapsulated amoxicillin.

The release of the drug increases from 32.7% to 96% over the 360 minutes, with an almost linear relationship. The results show that the keratin-TPP particles are suitable for drug delivery and allow a slow, complete, and controlled release within 6 hours. 80% of the initial drug concentration is released in about 300 minutes. This keratin-based delivery platform is ideal for short-term release with controlled, linear delivery and could be ideal for wound dressings. Due to its antioxidant activity, keratin is used as an anti-inflammatory agent in wound dressings as it reduces the possibility of bacterial infection, which prolongs wound healing.[15,21,27,51,67] Moreover, the fast initial

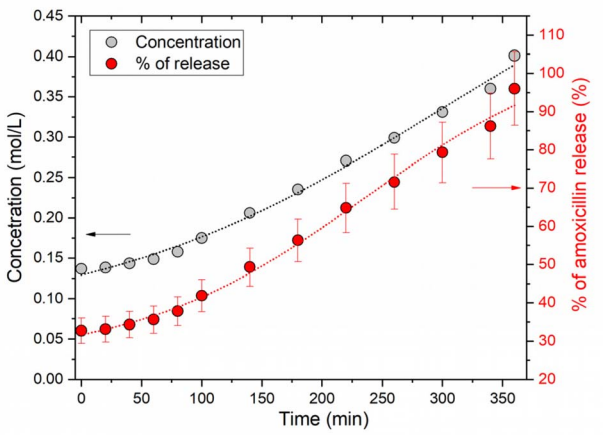

Fig. 5 Amoxicillin release from keratin-TPP nanoparticles.

release observed in this study could be particularly useful for acute wound infections, where rapid local antibiotic action is critical. For chronic wounds, a secondary formulation that modulates release kinetics may be needed.[76]

The antimicrobial and antioxidant activity of keratin-TPP particles with embedded antibiotic drug amoxicillin was also tested. When the drug amoxicillin was embedded in keratin-TPP nanoparticles, the antioxidant activity increased to 84.2% in 60 minutes (Fig. 6), indicating that amoxicillin contributes to antioxidant activity, and this system showed almost the same great antioxidant activity as keratin itself.

While amoxicillin is primarily known for its antibiotic properties, some research suggests that it may have additional effects, including potential antioxidant activity. Some studies have indicated that certain antibiotics, including amoxicillin, may exhibit antioxidant effects in specific contexts.[57] Our results (Fig. 6) of testing amoxicillin at the concentration at which it was encapsulated in the particles clearly demonstrate the excellent antioxidant activity of amoxicillin. Moreover,

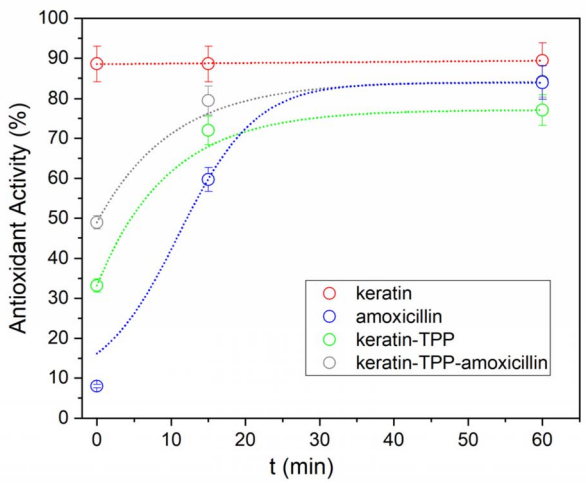

Fig. 6 Antioxidant activity of keratin-TPP-amoxicillin nanoparticles.

amoxicillin obviously works synergistically with keratin and helps to neutralise harmful free radicals.

In addition, keratin has been shown to have a higher drug loading capacity compared to other protein carriers such as albumin, allowing efficient encapsulation of amoxicillin while maintaining its therapeutic activity. The drug-loaded nanoparticles retain their bioactivity and ensure that the antibiotic remains effective for treatment.[27,77] Research shows that keratin nanoparticles can provide pH-dependent and sustained release profiles, which is important for antibiotics such as amoxicillin to maintain therapeutic effect over time and minimize dosing frequency. This controlled release can help to deliver the drug in a targeted manner and avoid premature degradation and side effects.[27]

Importantly, encapsulation in keratin nanoparticles can protect amoxicillin from enzymatic degradation and chemical instability in physiological environments, potentially increasing its half-life and bioavailability.

The zone inhibition with disk diffusion method is considered the gold standard for confirming the susceptibility of bacteria to antibiotics. It is widely used in clinical laboratories due to its simplicity, low cost and ability to screen for susceptibility to a larger number of antibiotics or an entire class of antibiotics.[58]

To monitor the antimicrobial activity of the keratin-based delivery platform keratin-TPP-amoxicillin, the zone inhibition test was performed against Gram-negative (*E. coli*) and Gram-positive bacteria (*S. aureus*). Fig. 7 shows the results for 4 samples: (1) pure amoxicillin, (2) pure keratin, (3) keratin-TPP nanoparticles and (4) keratin-TPP nanoparticles with encapsulated amoxicillin for both bacteria. As expected, only the samples containing amoxicillin exhibit antimicrobial activity against both *E. coli* and *S. aureus*, as indicated by the formation of an inhibition zone around the sample applied to the disks. Since no inhibition zone is formed when keratin (sample 2) or keratin-TPP nanoparticles (sample 3) are tested against both bacteria, it can be concluded that neither keratin nor TPP exhibit antimicrobial resistance.

The diameter of the inhibition zone for amoxicillin against *E. coli* (18.3 mm) is larger than that against *S. aureus* (12.7 mm) possibly reflecting differences in cell wall permeability or drug susceptibility. From this it can be concluded that Gram-positive bacteria are more resistant to amoxicillin. These results are consistent with the study conducted in Ethiopia, in which the mean zone of inhibition of amoxicillin against *E. coli* was determined to be 14.2 ± 4.0 mm.[59] Amoxicillin is generally effective against many strains of *E. coli.* However, antibiotic susceptibility can vary among different strains, and in cases of severe infections or when antibiotic resistance is a concern, healthcare providers may consider alternative antibiotics.[60] No results on the inhibition zone of amoxicillin against *S. aureus* were found in the literature. Amoxicillin may be effective against some strains of *S. aureus*, but many strains have developed resistance to this antibiotic, particularly those that produce an enzyme called beta-lactamase.[61] In cases of suspected *S. aureus* infections, healthcare providers often perform an antibiotic susceptibility test to determine whether amoxicillin is an appropriate treatment.

Since keratin and keratin-TPP nanoparticles exhibit no inhibition zone, the increased inhibition against both *E. coli* (22 mm) and *S. aureus* (15.3 mm) in sample 4 (keratin-based delivery platform keratin-TPP-amoxicillin) compared to pure amoxicillin (Fig. 8) can be attributed to the successful and controlled release of the drug from the particles, confirming that controlled drug release kinetics play a crucial role in its effectiveness and confirming that the antimicrobial effect is due to the released amoxicillin rather than inherent matrix activity. Similar inhibition zones have been reported in other keratin-based delivery systems containing antibiotics, typically ranging from 10–25 mm depending on the pathogen and formulation. The observed diameters in this study fall within

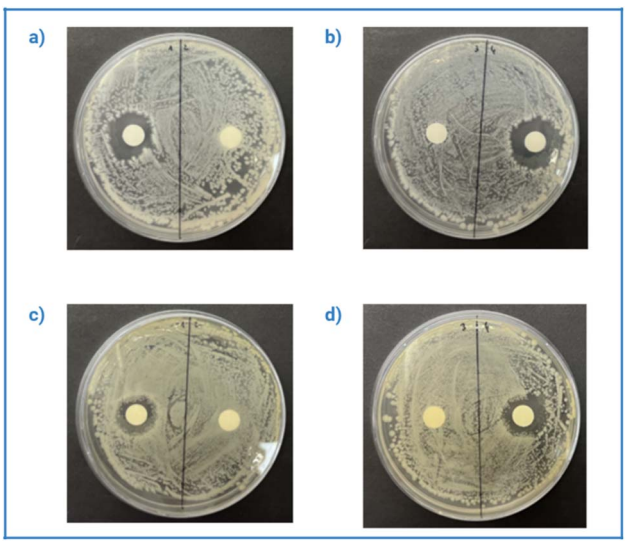

Fig. 7 The zone inhibition test against *E. coli* – Petri dishes (a) and (b), and against *S. aureus* – Petri dishes (c) and (d).

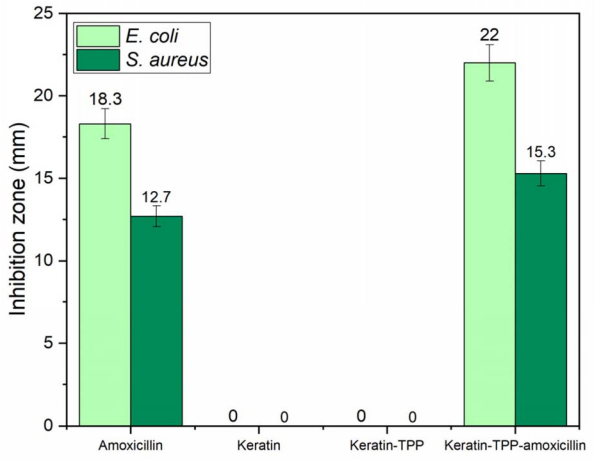

Fig. 8 The measured inhibition zone for amoxicillin, keratin, keratin-TPP and keratin-based delivery platform keratin-TPP-amoxicillin.

this effective range, indicating adequate release and preserved activity of the drug.[78]

Enhanced antioxidant and antimicrobial efficacy through keratin-amoxicillin synergy

The combination of amoxicillin with keratin-TPP nanoparticles demonstrates enhanced antimicrobial and antioxidant effects, which can be explained by multiple synergistic mechanisms. Firstly, it has been reported that keratin-based encapsulation may reduce drug exposure to degrading conditions and potentially improve apparent stability in complex environments.[27] Keratin's amphiphilic structure and high drug-loading capacity enable physical entrapment and electrostatic interaction with the β-lactam ring of amoxicillin, resulting in stable encapsulation and controlled release.[79]

Secondly, keratin contains cysteine residues with thiol (−SH) groups, which exhibit strong antioxidant activity by scavenging free radicals. This is particularly relevant in chronic wounds, where excessive ROS impair healing and promote bacterial persistence. By reducing oxidative stress, keratin may restore redox balance, protect surrounding tissues, and enhance the local efficacy of antibiotics.[80]

Thirdly, the nanoscale size (<500 nm) and surface charge of keratin-TPP particles facilitate better mucosal or dermal penetration and interaction with bacterial membranes, enhancing drug diffusion and uptake.[81] The sustained release observed over several hours supports continuous bactericidal concentrations at the infection site, reducing the likelihood of resistance development and improving overall therapeutic outcomes.

While amoxicillin itself may exhibit limited antioxidant properties in certain conditions, its co-delivery with keratin results in additive or synergistic antioxidant effects, as seen in increased ABTS scavenging in combined systems.

In summary, keratin-amoxicillin nanoparticles provide multifunctional benefits: physical protection, controlled/sustained drug release, ROS neutralization, and enhanced antimicrobial potency. This makes them a promising platform for applications such as wound dressings, local infection control, or antibiotic delivery systems.

It's worth noting that prior findings have demonstrated that hydrolysed keratin poses no toxicity concerns, even upon double dilution, and additionally, it promotes the growth of epithelial cells.[70] In the case of TPP, it's generally regarded as safe for use in food products and finds various applications across different industries. Importantly, the concentration of TPP utilized in keratin-TPP nanoparticles is so minimal that it does not elicit toxicity, as corroborated by the study conducted by Ristić *et al.*[63]

Conclusions

This study highlights the potential of keratin extracted from poultry feathers *via* subcritical water (SubCW) processing as a sustainable and environmentally friendly resource for advanced biomedical applications. The SubCW approach eliminates the need for toxic organic solvents, maintains the molecular integrity of keratin, and yields pharmaceutical-grade material suitable for incorporation into medical and biomedical formulations. By converting feather-derived keratin into well-defined micro- and nanoscale particles in combination with functional polyelectrolytes such as alginate, chitosan, and especially tripolyphosphate (TPP), it is possible to tailor structural and functional properties to meet specific therapeutic requirements.

Among the tested systems, keratin particles crosslinked with TPP exhibited the highest structural stability, biocompatibility, drug encapsulation efficiency, and controlled release behaviour, as demonstrated using amoxicillin as a model drug. The ionic crosslinking approach with TPP, despite the small molecular size of the crosslinker, proved effective in creating robust keratin-based nanocarriers. These systems differ significantly in their interaction mechanisms and functional outcomes from conventional polyelectrolyte-based nanoparticles, offering opportunities to design delivery platforms for targeted biomedical applications. Importantly, keratin-TPP particles demonstrated multifunctionality by combining potent antioxidant activity with broad-spectrum antimicrobial properties against both Gram-positive and Gram-negative bacteria, thereby contributing actively to therapeutic action in addition to drug transport.

The versatility of these particles extends beyond direct administration, as their favourable physicochemical and bioactive properties make them ideal candidates for integration into advanced wound care platforms such as hydrogels, creams, or dressing matrices. This dual functionality—serving as both drug carriers and active therapeutic agents—positions keratin-TPP complexes as a competitive alternative to conventional delivery systems. The present work therefore provides a strong proof of concept for the development of next-generation biomedical materials based on bio-derived, safe, and functional components.

Future research should focus on fine-tuning formulation strategies to optimise drug loading, release kinetics, and stability, while expanding the range of therapeutic agents investigated. Comprehensive *in vivo* studies in relevant wound healing and infection models will be essential to confirm clinical efficacy and support translation toward medical and veterinary applications. Overall, the results of this study demonstrate not only the feasibility of upcycling poultry feather keratin into high-value, multifunctional micro/nanoparticles but also their potential as sustainable, effective, and practical platforms for antibiotic delivery and advanced biomedical material design.

Author contributions

Fras Zemljič: conceptualisation, supervision, investigation, methodology, writing original draft, draft review & editing; Tušek: writing original draft, draft review & editing; Mešl: investigation, methodology; Plohl: conceptualisation, supervision, investigation, methodology, writing original draft, draft review & editing; Čolnik: conceptualisation, supervision, draft review & editing; Škerget: conceptualisation, supervision,

investigation, methodology, writing original draft, draft review & editing.

Conflicts of interest

The Authors declare that they have no known competing financial interests or personal relationship that could have appeared to influence the work reported in this paper.

Data availability

All data supporting the findings of this study are available within the article. The detailed data are available at main author.

Acknowledgements

The authors would like to acknowledge financial support from the Slovenian Research Agency (research project J7-4492, and Programme groups P2-0118, P2-0421 and P2-0414).

References

1 A. R. Seidavi, H. Zaker-Esteghamati and C. G. Scanes, *Worlds. Poult. Sci. J.*, 2019, **75**, 55–68, DOI: 10.1017/S0043933918000764.
2 N. C. Barman, F. T. Zohora, K. C. Das, M. G. Mowla, N. A. Banu, M. Salimullah and A. Hashem, *AMB Express*, 2017, **7**, 181, DOI: 10.1186/s13568-017-0462-6.
3 I. C. Ossai, S. Hamid and A. Hassan, *Waste Manage.*, 2022, **151**, 81–104, DOI: 10.1016/j.wasman.2022.07.021.
4 N. Prasanthi, S. Bhargavi and P. V. S. Machiraju, *Int. J. Innov. Res. Sci. Technol.*, 2016, **5**, 16759–16764.
5 Why bother with feather waste?, https://unlock-project.eu/why-bother-with-feather-waste/, accessed February 2026.
6 T. Mcgauran, M. Harris, N. Dunne, B. M. Smyth and E. Cunningham, *ACS Sustain. Chem. Eng.*, 2022, **10**, 486–494, DOI: 10.1021/acssuschemeng.1c06791.
7 C. R. Chilakamarry, S. Mahmood, S. N. B. M. Saffe, M. A. Bin Arifin, A. Gupta, M. Y. Sikkandar, S. S. Begum and B. Narasaiah, *3 Biotech*, 2021, **11**, 1–12, DOI: 10.1007/s13205-021-02734-7.
8 A. Idris, R. Vijayaraghavan, U. A. Rana, D. Fredericks, A. F. Patti and D. R. Macfarlane, *Green Chem.*, 2013, **15**, 525–534.
9 M. Brebu and I. Spiridon, *J. Anal. Appl. Pyrolysis*, 2011, **91**, 288–295.
10 P. Staroń, M. Banach, Z. Kowalski and A. Staroń, *Proc. ECOpole*, 2014, **8**, 443–448.
11 Y. Ji, J. Chen, J. Lv, Z. Li, L. Xing and S. Ding, *Sep. Purif. Technol.*, 2014, **132**, 577–583, DOI: 10.1016/j.seppur.2014.05.049.
12 S. Ding, Y. Sun, H. Chen, C. Xu and Y. Hu, *Chin. J. Chem. Eng.*, 2019, **27**, 660–667.
13 A. Shavandi, A. Carne, A. A. Bekhit and A. E.-D. A. Bekhit, *J. Environ. Chem. Eng.*, 2017, **5**, 1977–1984.
14 I. Sinkiewicz, H. Staroszczyk and I. Kołodziejska, *Waste Biomass Valorization*, 2017, **8**, 1043–1048, DOI: 10.1007/s12649-016-9678-y.
15 S. Feroz, N. Muhammad, J. Ranayake and G. Dias, *Bioact. Mater.*, 2020, **5**, 496–509, DOI: 10.1016/J.BIOACTMAT.2020.04.007.
16 T. Rogalinski, K. Liu, T. Albrecht and G. Brunner, *J. Supercrit. Fluids*, 2008, **46**, 335–341, DOI: 10.1016/j.supflu.2007.09.037.
17 V. Alexandru FARAON, E. Gabriela MIHĂILĂ, N. Tritean, B. Trică, L. Capră, M.-B. Roman, D. Constantinescu-aruxandei and F. Oancea, *Sci. Bull. Ser. F. Biotechnol.*, 2023, **XXVII**, 105–112.
18 M. Škerget, M. Čolnik, L. F. Zemljič, L. Gradišnik, T. Ž. Semren, B. T. Lovaković and U. Maver, *Polymers*, 2023, **15**, 1–15, DOI: 10.3390/polym15122658.
19 A. Verdnik, M. Čolnik, Ž. Knez and M. Škerget, *Acta Chim. Slov.*, 2021, **68**, 433–440, DOI: 10.17344/acsi.2020.6538.
20 Data Bridge Market Research, *Keratin Market – Global Industry Trends and Forecast to 2029*, 2022.
21 S. Sharma, H. Rostamabadi, S. Gupta, A. Kumar Nadda, M. S. Kharazmi and S. M. Jafari, *Eur. Polym. J.*, 2022, **180**, 111614, DOI: 10.1016/J.EURPOLYMJ.2022.111614.
22 S. S. Dhilip Kumar and H. Abrahamse, *Front. Chem.*, 2022, **10**, 969809.
23 N. Kučuk, M. Primožič, Ž. Knez and M. Leitgeb, *Int. J. Mol. Sci.*, 2023, **24**, 3188.
24 A. V Samrot, T. C. Sean, T. Kudaiyappan, U. Bisyarah, A. Mirarmandi, A. Abubakar, H. H. Ali, J. L. A. Angalene and S. S. Kumar, *Int. J. Biol. Macromol.*, 2020, **165**, 3088–3105.
25 S. M. H. Hosseini, F. Ghiasi, and M. Jahromi, Nanocapsule formation by complexation of biopolymers, in *Nanoencapsulation technologies for the food and nutraceutical industries*, ed. S. M. Jafari, Academic Press, 2017, pp. 447–492.
26 A. Wilson, E. E. Ekanem, D. Mattia, K. J. Edler and J. L. Scott, *ACS Sustain. Chem. Eng.*, 2021, **9**, 16617–16626, DOI: 10.1021/acssuschemeng.1c05304.
27 C. Ferroni and G. Varchi, *Appl. Sci.*, 2021, **11**(20), 9417, DOI: 10.3390/app11209417.
28 F. Ahmadi, Z. Oveisi, M. Samani and Z. Amoozgar, *Res. Pharm. Sci.*, 2015, **10**, 1–16.
29 C. W. Lin, Y. K. Chen, M. Lu, K. L. Lou and J. Yu, *Polymers*, 2018, **10**(9), 987, DOI: 10.3390/polym10090987.
30 F. Abasalizadeh, S. V. Moghaddam, E. Alizadeh, E. Akbari, E. Kashani, S. M. B. Fazljou, M. Torbati and A. Akbarzadeh, *J. Biol. Eng.*, 2020, **14**, 1–22, DOI: 10.1186/s13036-020-00239-0.
31 S. Iravani and R. Varma, *Mar. Drugs*, 2022, **20**, 598, DOI: 10.3390/md20100598.
32 F. G. de Carvalho, T. C. Magalhães, N. M. Teixeira, B. L. C. Gondim, H. L. Carlo, R. L. dos Santos, A. R. de Oliveira and Â. M. L. Denadai, *Mater. Sci. Eng. C*, 2019, **104**, 109885, DOI: 10.1016/j.msec.2019.109885.
33 S. Sreekumar, F. M. Goycoolea, B. M. Moerschbacher and G. R. Rivera-Rodriguez, *Sci. Rep.*, 2018, **8**(1), 4695, DOI: 10.1038/s41598-018-23064-4.

34 A. R. Cho, Y. G. Chun, B. K. Kim and D. J. Park, *J. Food Sci.*, 2014, **79**(4), E568–E576, DOI: 10.1111/1750-3841.12395.
35 E. M. A. Hejjaji, A. M. Smith and G. A. Morris, *Int. J. Biol. Macromol.*, 2018, **120**, 1610–1617, DOI: 10.1016/j.ijbiomac.2018.09.185.
36 C. Pan, J. Qian, C. Zhao, H. Yang, X. Zhao and H. Guo, *Carbohydr. Polym.*, 2020, **241**, 116349, DOI: 10.1016/j.carbpol.2020.116349.
37 T. K. Glaser, O. Plohl, A. Vesel, U. Ajdnik, N. P. Ulrih, M. K. Hrnčič, U. Bren and L. F. Zemljič, *Materials*, 2019, **12**(13), 2118, DOI: 10.3390/ma12132118.
38 S. Potrč, L. F. Zemljič, M. Sterniša, S. S. Možina and O. Plohl, *Int. J. Mol. Sci.*, 2020, **21**(10), 3668, DOI: 10.3390/ijms21103668.
39 D. Čakara, L. Fras, M. Bračič and K. S. Kleinschek, *Carbohydr. Polym.*, 2009, **78**, 36–40.
40 S. Sharma, A. Gupta, S. Mohd Saufi Tuan Chik, C. Yeo Gek Kee, P. Kumar Podder, J. Thraisingam, and M. Subramaniam, *Proc. Natl. Conf. Postgrad. Res. (NCON-PGR 2016)*, Univ. Malaysia Pahang (UMP), Pekan, 2026, pp. 693–699.
41 C. Sartori, D. S. Finch, B. Ralph and K. Gilding, *Polymer*, 1997, **38**, 43–51, DOI: 10.1016/S0032-3861(96)00458-2.
42 R. Pereira, A. Tojeira, D. C. Vaz, A. Mendes and P. Bártolo, *Int. J. Polym. Anal. Charact.*, 2011, **16**, 449–464.
43 Z. Wang, H. Yang and Z. Zhu, *Polymer*, 2019, **163**, 144–153.
44 Y. Srisuwan and P. Srihanam, *Adv. Mater. Sci. Eng.*, 2018, **2018**(1), 8129218, DOI: 10.1155/2018/8129218.
45 A. Arafat, S. A. Samad, S. M. Masum and M. Moniruzzaman, *Int. J. Sci. Eng. Res.*, 2015, **6**, 538–541.
46 M. R. Kasaai, *J. Agric. Food Chem.*, 2009, **57**, 1667–1676, DOI: 10.1021/jf803001m.
47 X. Wang, Z. Shi, Q. Zhao and Y. Yun, *Materials*, 2021, **14**, 379, DOI: 10.3390/ma14020379.
48 A. Barth, *Prog. Biophys. Mol. Biol.*, 2000, **74**, 141–173, DOI: 10.1016/S0079-6107(00)00021-3.
49 A. Ferreira Tomaz, S. M. Sobral de Carvalho, R. Cardoso Barbosa, S. M. L. Silva, M. A. Sabino Gutierrez, A. G. B. de Lima and M. V. L. Fook, *Materials*, 2018, **11**, 2051.
50 M. Hidaka, M. Kojima, S. Sakai and C. Delattre, *Polymers*, 2024, **16**, 1274, DOI: 10.3390/polym16091274.
51 E. Alehosseini, S. Tabarestani, H. Kharazmi, E. Alehosseini, H. S. Tabarestani, M. S. Kharazmi and S. M. Jafari, *Foods*, 2022, **11**, 3841–11, DOI: 10.3390/foods11233841.
52 I. Silvestro, I. Francolini, V. Di Lisio, A. Martinelli, L. Pietrelli, A. S. d'Abusco, A. Scoppio and A. Piozzi, *Mater*, 2020, **13**, 3577, DOI: 10.3390/MA13163577.
53 M. Gierszewska and J. Ostrowska-Czubenko, *Carbohydr. Polym.*, 2016, **153**, 501–511, DOI: 10.1016/j.carbpol.2016.07.126.
54 I. G. Munteanu and C. Apetrei, *Int. J. Mol. Sci.*, 2021, **22**(7), 3380, DOI: 10.3390/ijms22073380.
55 F. Salvo, A. De Sarro, A. P. Caputi and G. Polimeni, *Expert Opin. Drug Saf.*, 2009, **8**, 111–118, DOI: 10.1517/14740330802527984.
56 M. Konop, M. Rybka and A. Drapała, *Pharmaceutics*, 2021, **13**(12), 2029, DOI: 10.3390/pharmaceutics13122029.
57 M. M. Abd El-Emam, M. Mostafa, A. A. Farag, H. S. Youssef, A. S. El-Demerdash, H. Bayoumi, M. A. Gebba, S. M. El-Halawani, A. M. Saleh and A. M. Badr, *Antioxidants*, 2023, **12**, 1487.
58 M. Xing, C. Qi, W. Yu, X. Han, Z. Jiarui, Z. Qing, J. Aiguo and S. Shuliang, *Mar. Drugs*, 2020, **18**, 144, DOI: 10.3390/md18030144.
59 D. Demissie, T. Geremew, A. Z. Chernet and M. M. Ali, *PLoS One*, 2021, **16**(7), e0253971, DOI: 10.1371/journal.pone.0253971.
60 S. A. Jafri, M. Qasim, M. S. Masoud, M.-U. - Rahman, M. Izhar and S. Kazmi, *Bioinformation*, 2014, **10**, 419–422, DOI: 10.6026/97320630010419.
61 F. C. Groppo, F. M. Castro, A. B. Pacheco, R. H. Motta, T. R. de M. Filho, J. C. Ramacciato, F. M. Florio and J. G. Meechan, *Gen. Dent.*, 2005, **53**, 410–413.
62 C. L. Burnett, W. F. Bergfeld, D. V Belsito, R. A. Hill, C. D. Klaassen, D. C. Liebler, J. G. Marks, R. C. Shank, T. J. Slaga, P. W. Snyder, *et al.*, *Int. J. Toxicol.*, 2021, **40**, 36S–51S, DOI: 10.1177/10915818211013019.
63 T. Ristić, S. Lasič, I. Kosalec, M. Bračič and L. Fras-Zemljič, *React. Funct. Polym.*, 2015, **97**, 56–62.
64 P. Calvo, C. Remuñan-López, J. L. Vila-Jato and M. J. Alonso, *Pharm. Res.*, 1997, **14**(10), 1431–1436, DOI: 10.1023/A:1012128907225.
65 Q. Gan and T. Wang, *Colloids Surf., B*, 2007, **59**(1), 24–34, DOI: 10.1016/j.colsurfb.2007.04.009.
66 M. Sheikh Hosseini, Z. Moosavi-Nejad, F. Rezaei Sadrabadi and H. Hosano, *Int. J. Mol. Sci.*, 2025, 4149–26, DOI: 10.3390/ijms26094149.
67 L. Zheng, M. Zhao, C. Xiao, Q. Zhao and G. Su, *Food Chem.*, 2016, **192**, 288–294, DOI: 10.1016/j.foodchem.2015.07.015.
68 L. Bugnicourt and C. Ladavière, *Prog. Polym. Sci.*, 2016, **60**, 1–17, DOI: 10.1016/j.progpolymsci.2016.06.002.
69 J. MatyaSovsky, J. Sedliačik, K. Valachová, I. Novák, P. Jurkovič, P. Duchovič, M. Mičušik, A. Kleinová, L. Šoké and J. Am. Leather, *Chem. Assoc.*, 2017, **112**, 327–337.
70 S. Sharma, A. Gupta, S. M. S. T. Chik, C. G. Kee, B. M. Mistry, D. H. Kim and G. Sharma, *Int. J. Biol. Macromol.*, 2017, **104**, 189–196, DOI: 10.1016/J.IJBIOMAC.2017.06.015.
71 Y. Dong and Z. Wang, *ROS-Scavenging Materials for Skin Wound Healing: Advancements and Applications*, 2023, DOI: 10.3389/fbioe.2023.1304835.
72 I. Ammendolia, C. Mannucci, E. Esposito, G. Calapai, M. Currò, P. Midiri, L. Cardia and F. Calapai, *Molecules*, 2025, **30**, 3825, DOI: 10.3390/MOLECULES30183825.
73 K. K. Sodhi, M. Kumar and D. K. Singh, *J. Water Process Eng.*, 2021, **39**, 101858, DOI: 10.1016/j.jwpe.2020.101858.
74 L. Nong, X. Liu, X. Wang, W. de Leeuw, M. Jonker, S. Brul and B. ter Kuile, *Antimicrob. Agents Chemother.*, 2025, **69**(9), e0044125, DOI: 10.1128/aac.00441-25.
75 M. Zhai, Y. Xu, B. Zhou and W. Jing, *J. Photochem. Photobiol. B Biol.*, 2018, **180**, 253–258, DOI: 10.1016/j.jphotobiol.2018.02.018.
76 J. Hurlow and P. G. Bowler, *Acute and Chronic Wound Infections: Microbiological, Immunological, Clinical and*

Therapeutic Distinctions, 2022, DOI: 10.12968/jowc.2022.31.5.436.

77 E. Martella, C. Ferroni, A. Guerrini, M. Ballestri, M. Columbaro, S. Santi, G. Sotgiu, M. Serra, D. M. Donati and E. Lucarelli, *Int. J. Mol. Sci.*, 2018, **19**(11), 3670, DOI: 10.3390/ijms19113670.

78 M. Sundaram, R. Legadevi, A. N. Banu, V. Gayathri and A. Palanisammy, *Eur. J. Biotechnol. Biosci.*, 2015, **6**, 1–5.

79 A. Aluigi, M. Ballestri, A. Guerrini, G. Sotgiu, C. Ferroni, F. Corticelli, M. B. Gariboldi, E. Monti and G. Varchi, *Mater. Sci. Eng. C*, 2018, **90**, 476–484, DOI: 10.1016/j.msec.2018.04.088.

80 M. Pakdel, Z. Moosavi-Nejad, R. K. Kermanshahi and H. Hosano, *J. Clean. Prod.*, 2022, **335**, 130331, DOI: 10.1016/j.jclepro.2021.130331.

81 J. Wang, S. Hao, T. Luo, Q. Yang and B. Wang, *Mater. Sci. Eng. C*, 2016, **68**, 768–773, DOI: 10.1016/j.msec.2016.07.035.